

Numerical analysis of tunnel in rock with basalt fiber reinforced concrete lining subjected to internal blast load

Priyanka Jain^a and Tanusree Chakraborty*

Department of Civil Engineering, Indian Institute of Technology (IIT) Delhi, Hauz Khas, New Delhi, 110 016, India

(Received April 22, 2017, Revised November 17, 2017, Accepted December 4, 2017)

Abstract. The present study focuses on the performance of basalt fiber reinforced concrete (BFRC) lining in tunnel situated in sandstone rock when subjected to internal blast loading. The blast analysis of the lined tunnel is carried out using the three-dimensional (3-D) nonlinear finite element (FE) method. The stress-strain response of the sandstone rock is simulated using a crushable plasticity model which can simulate the brittle behavior of rock and that of BFRC lining is analyzed using a damaged plasticity model for concrete capturing damage response. The strain rate dependent material properties of BFRC are collected from the literature and that of rock are taken from the authors' previous work using split Hopkinson pressure bar (SHPB). The constitutive model performance is validated through the FE simulation of SHPB test and the comparison of simulation results with the experimental data. Further, blast loading in the tunnel is simulated for 10 kg and 50 kg Trinitrotoluene (TNT) charge weights using the equivalent pressure-time curves obtained through hydrocode simulations. The analysis results are studied for the stress and displacement response of rock and tunnel lining. Blast performance of BFRC lining is compared with that of plain concrete (PC) and steel fiber reinforced concrete (SFRC) lining materials. It is observed that the BFRC lining exhibits almost 65% lesser displacement as compared to PC and 30% lesser displacement as compared to SFRC tunnel linings.

Keywords: blast; basalt fiber reinforced concrete; split hopkinson pressure bar; tunnel lining

1. Introduction

Underground facilities are used extensively for public transportation, water and sewage conveyance and storage of petroleum and ammunition. An explosion inside an underground infrastructure may pose a direct threat to the lives of people inside it by causing damage to the steel or concrete lining and the heavy support system. Moreover, the loss encountered due to the blast induced destruction of properties is massive. Hence, the design of underground infrastructure deserves proper attention in terms of selection of the tunnel lining material which can sustain the blast induced energy (Chakraborty *et al.* 2014). In the literature, many studies have been performed in the simulation of blast loading in underground infrastructure (Hao *et al.* 1998, Choi *et al.* 2006, Liu 2009, Tiwari *et al.* 2014, Tiwari 2015, Yu *et al.* 2015, Zhao *et al.* 2017). Hao *et al.* (1998) used a continuum damage model for simulating failure of rock in analyzing the damaged zone due to underground explosions through numerical simulations. Rock was assumed as an isotropic homogeneous and continuous medium in their investigations. Choi *et al.* (2006) studied the deformation in the concrete lining due to blast pressure using 3-D FE methods for different explosive parameters. Dynamic response and damage of subway structures in soil are

analyzed by Liu (2009) where explosive loading was modeled using CONWEP reflected pressure and applied to the tunnel lining as impulse loading. Significant deformation of soil was observed. It was concluded that ground stiffness has a significant influence on lining stress and damage of the lining. Tiwari (2015) analyzed tunnels in soil and rock with reinforced concrete tunnel lining for internal blast load and showed that both the lining and the surrounding geological material undergo significant damage when subjected to blast loading. Yu *et al.* (2015) developed a fully coupled numerical model to simulate dynamic response of tunnel structure in soil under internal blast load and observed that the tunnel responses are driven by tunnel stiffness and location of charge. Vibration analysis of a cylindrical tunnel due to blast load was done by Zhao *et al.* (2017). It is noted from the literature review that for blast resistant design of underground structures, it is necessary to use more ductile energy absorbing materials as tunnel lining. In the present work, the performance of basalt fiber reinforced concrete (BFRC) in tunnel lining and its blast performance will be studied which has not been explored so far.

The basalt fiber, which is mixed with concrete for increasing the ductility and energy absorbing properties of concrete, is made from crushed basalt rock melted at nearly 1,400°C (2,550°F). The molten rock is then extruded through small nozzles to produce continuous filaments of basalt fiber. They are environmentally safe and non-toxic, possess high heat stability and are crack resistant (Ramakrishnan *et al.* 1998, Girgin and Yildirim 2015, Zhang *et al.* 2015, Arslan 2016, Ganesan *et al.* 2017). Unlike steel fiber in concrete, basalt fibers have not been

*Corresponding author, Associate Professor
E-mail: tanusree@civil.iitd.ac.in

^aM. Tech. Student
E-mail: priyankagwalior.jain@gmail.com

widely used, possibly due to lack of research and extensive testing required. Li and Xu (2009) performed split Hopkinson pressure bar (SHPB) experiments on the BFRC at different strain rates and observed that addition of basalt fiber in concrete can significantly improve deformation and energy absorption properties of concrete. The specific objective of the present work is to study the effectiveness of the BFRC lining in the tunnels when subjected to internal blast loading through 3-D nonlinear FE analysis, for the first time in the literature. In the present work, blast analysis of tunnels in sandstone rock with BFRC lining are performed using the FE software Abaqus/Explicit (Abaqus manual version 6.11) and the results are studied for stresses and displacements in the lining and the surrounding rock. The stress-strain response of sandstone rock is analysed using the crushable foam plasticity model which can simulate the brittle behavior of rock and the stress-strain response of BFRC lining is simulated using the concrete damaged plasticity model capturing the damage response of concrete. The strain rate dependent material properties of BFRC are collected from the literature and that of rock is taken from the authors' previous works. The constitutive model performance for BFRC is validated by simulating SHPB test using the FE method and comparing the simulation results with the experimental data reported in Li and Xu (2009). Further, FE simulation of tunnels in sandstone rock with BFRC lining subjected to internal blast load induced by 10 kg and 50 kg TNT is performed. The stresses and displacements in the BFRC lining and rock are compared with that of plain concrete (PC) and steel fiber reinforced concrete (SFRC) tunnel linings and the differences in the lining and rock response under blast loading are reported.

Table 1 Physical and mechanical properties of short basalt fiber (Choi *et al.* 2006)

Filament Diameter (μm)	Length (mm)	Density (kg/m^3)	Tensile Modulus (GPa)	Tensile Strength (MPa)	Elongation at Break (%)
7-15	18	2650	93-110	4150-4800	3.1-3.3

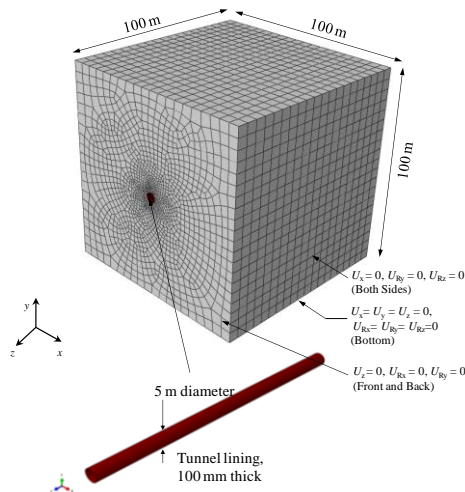


Fig. 1 Model geometry and meshed basalt fiber reinforced concrete tunnel lining

2. Three dimensional finite element model

2.1 Mesh and boundary conditions

The three-dimensional (3-D) nonlinear finite element (FE) analyses of tunnels subjected to internal blast load are analyzed herein using FE software Abaqus/Explicit. A 5 m diameter tunnel in the soft sandstone rock with 100 mm thick BFRC lining is considered in the analyses. Fig. 1 shows the model geometry and boundary conditions considered herein. The tunnel is located at a depth of 50 m below the ground surface. The length, breadth, and width of the FE model are taken as 100 m each. The model dimensions are chosen in such a way that sufficient rock domain around the tunnel remains in place and the domain boundaries do not affect the results of the analyses. The horizontal surface at the bottom of the domain is kept fixed in all Cartesian directions ($U_x=U_y=U_z=0$), while the top horizontal boundary is free to deform. The left and right vertical boundaries are restrained in horizontal directions, however, free to move in vertical direction. The rock mass and lining are discretized using three-dimensional eight node linear brick element with reduced integration and hourglass control (C3D8R). Fig. 1 shows the 3-D mesh of rock mass, tunnel, and basalt fiber reinforced concrete lining. The interface between tunnel lining and rock is modeled using the general contact algorithm available in Abaqus with hard contact in the normal direction and frictional contact in the tangential direction. Validation of finite element model is presented in other manuscripts by the same author (Tiwari *et al.* 2016, Khan *et al.* 2016) and thus, has not been included in the current manuscript.

2.2 Constitutive models and material properties

In the present work, strain rate-dependent constitutive models have been used to simulate the stress-strain response of both concrete materials and rock as blast load gives rise to high strain rate (10^2 - 10^4 /sec). The stress-strain response of BFRC, PC and SFRC are simulated using strain rate-dependent concrete damaged plasticity model. The yield function in the concrete damaged plasticity model is given by Lubliner *et al.* (1989) and later modified by Lee and Fenves (1998), as

$$F = \left(\sqrt{3/2} \sqrt{\bar{s} : \bar{s}} \right) - 3\alpha\bar{p} + \beta \left\langle \frac{\hat{\sigma}_{\max}}{\sigma_c} \right\rangle - \gamma \left\langle -\frac{\hat{\sigma}_{\max}}{\sigma_c} \right\rangle - (1-\alpha)\bar{\sigma}_c = 0 \quad (1)$$

where

$$\alpha = \frac{(\sigma_{b0}/\sigma_{c0}) - 1}{2(\sigma_{b0}/\sigma_{c0}) - 1} \quad (2)$$

$$\beta = \frac{\bar{\sigma}_c}{\bar{\sigma}_t} (1-\alpha) - (1+\alpha) \quad (3)$$

$$\gamma = \frac{3(1-K_c)}{2K_c - 1} \quad (4)$$

$$\bar{\sigma}_c = \frac{\sigma_c}{(1-d_t)} \quad (5)$$

$$\bar{\sigma}_t = \frac{\sigma_t}{(1-d_t)} \quad (6)$$

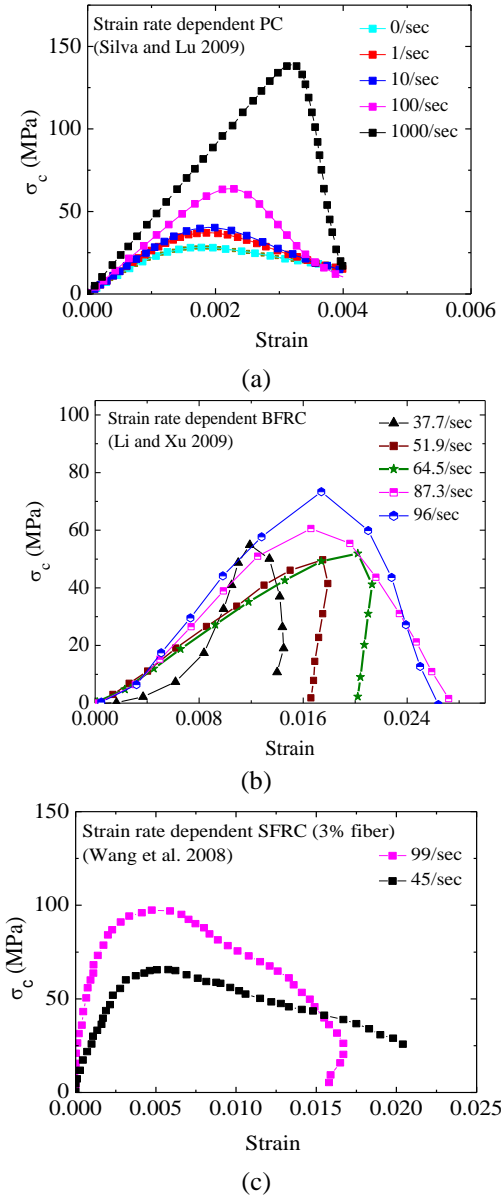


Fig. 2 Strain rate dependent stress-strain responses of (a) PC, (b) BFRC and (c) SFRC

where $\hat{\sigma}_{\max}$ is the maximum principal effective stress; $\bar{\sigma}$ is the deviatoric stress tensor; σ_{b0}/σ_{c0} is the ratio of initial equibiaxial compressive yield stress to initial uniaxial compressive yield stress; d_i is the damage variable and K_c is the ratio of the second deviatoric stress invariant on the tensile meridian to that on the compressive meridian at initial crushing for any given value of effective mean stress, $\bar{p} = (\bar{\sigma}_1 + \bar{\sigma}_2 + \bar{\sigma}_3)/3$. The concrete damaged plasticity model assumes a non-associated plastic flow rule.

The material properties of concrete damaged plasticity model for PC, BFRC, and SFRC are obtained from Silva and Lu (2009) for PC, Li and Xu (2009) for BFRC and Wang *et al.* (2008) for SFRC. Figs. 2(a), 2(b) and 2(c) show the strain rate dependent stress-strain response of PC, BFRC, and SFRC, respectively. It may be noted that although the three figures show different ranges of strain

Table 2 Physical and mechanical properties of plain concrete, basalt fiber reinforced concrete and steel fiber reinforced concrete

Material	Density ρ (kg/m ³)	Young's Modulus E (GPa)	Poisson's Ratio ν	Yield Strength (MPa)	References
PC	2643	27.38	0.2	$\sigma_c=2.0$, $\sigma_t=0.52$	Silva and Lu (2009) Dong <i>et al.</i> (2006),
BFRC	2880	29	0.2	$\sigma_c=6.7$, $\sigma_t=3.7$	Li and Xu (2009), Jalasatram <i>et al.</i> (2016)
SFRC	2880	34.6	0.2	$\sigma_c=4.0$, $\sigma_t=1.0$	Pawade <i>et al.</i> (2011), Wang <i>et al.</i> (2008)

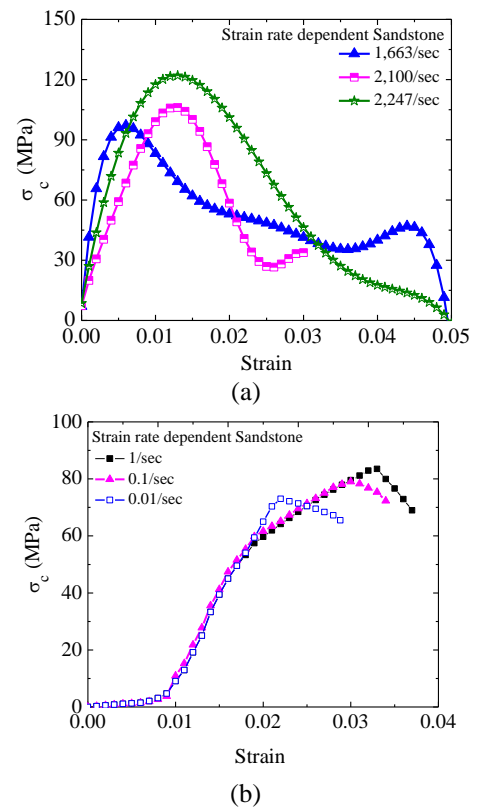


Fig. 3 Strain rate dependent stress-strain responses of sandstone at (a) high strain rate loading in SHPB test and (b) low strain rate loading in UTM test

rates, however, Abaqus interpolates the peak stress as per the strain rate developed in an analysis. The physical properties and yield strength of PC, BFRC and SFRC are reported in Table 2. In the present work, the mass density of BFRC and SFRC are assumed to be same as no data is available in the literature.

The crushable foam plasticity model is used to simulate the strain rate-dependent stress-strain response of sandstone. The yield surface of the model takes an elliptical shape in the mean stress (p) vs. deviatoric stress (q) plane. Inside the yield surface, the behavior of the foams remains linear elastic. The yield function is given by Deshpande and Fleck (2000) as

Table 3 Physical and mechanical properties of sandstone rock

Rock Type	Mass Density ρ (kg/m ³)	Young's Modulus E (GPa)	Poisson's Ratio (ν)	Yield Strength σ_y (MPa)	Reference
Sandstone	2291	13.6	0.35	23	Chakraborty (2013)

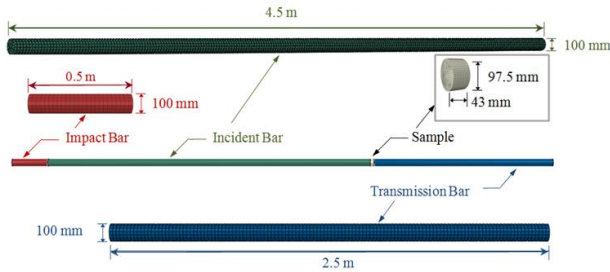


Fig. 4 Parts of SHPB in Abaqus

$$F = \sqrt{q^2 + \alpha^2(p - p_0)^2} - B = 0 \quad (7)$$

where p_0 is given by $(p_c - p_t)/2$; p_c and p_t are the yield strength values of the foam material under hydrostatic compression and tension, respectively. The parameter B is the magnitude of the intercept of yield surface with the vertical axis for deviatoric stress q ; and the parameter α defines the shape of the yield surface in the meridional plane. The volumetric hardening of the model is defined by providing the experimental data for uniaxial compressive strength with axial strain.

The constitutive model uses a non-associated flow rule. Physical properties and yield strength of sandstone rock are given in Table 3. The strain rate dependent stress-strain response of sandstone is presented in Fig. 3(a) for SHPB test (Mishra *et al.* 2015) and in Fig. 3(b) for universal testing machine (UTM) test (Alam *et al.* 2014) performed in TBRL, Chandigarh. The strain rate dependence of rock is included in the constitutive model by defining the strain rate dependent stress-strain response directly in the simulation.

The efficiency of the concrete damaged plasticity model in simulating strain rate dependent stress-strain response is checked by simulating SHPB tests on BFRC and comparing the stress-strain results obtained from simulation with the experimental data reported in Li and Xu (2009). The SHPB bar dimensions and the FE mesh considered for BFRC simulation are given in Fig. 4. The stress-strain response of BFRC as obtained from numerical simulation and its comparison with the experimental data are presented in Fig. 5 for different strain rates. It may be observed from Figs. 5(a) and 5(b) that the simulation results are comparing with the experimental data with reasonable accuracy. The efficiency of the crushable foam plasticity model in simulating strain rate dependent stress-strain response of rock was checked by Chakraborty (2013) for different rock types and not presented herein.

2.3 Blast simulation in tunnel

According to the recommendations of the Federal

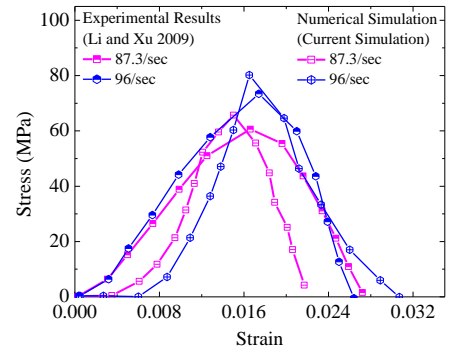
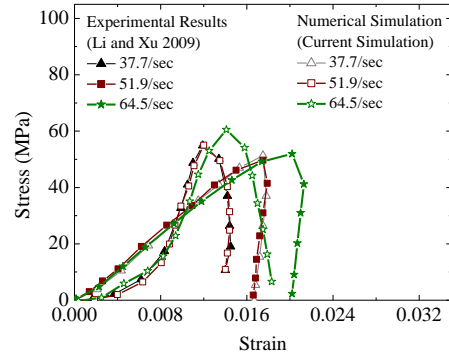


Fig. 5 Comparison of simulation and experimental results of SHPB test on BFRC at different strain rates

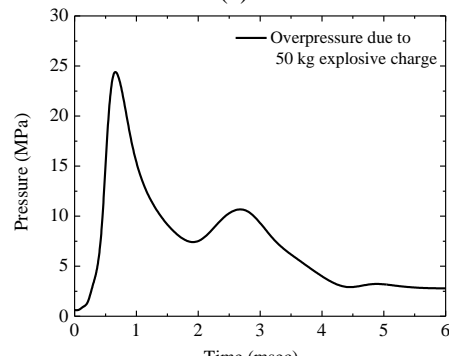
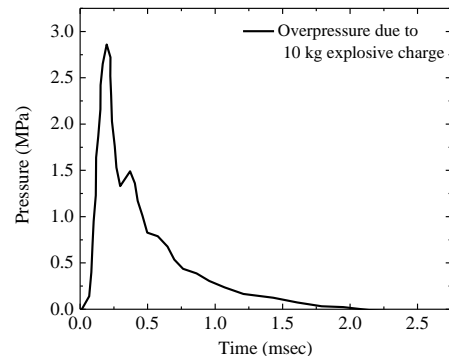


Fig. 6 Blast load profile due to (a) 10 kg TNT and (b) 50 kg TNT on the inner surface of tunnel lining

Emergency Management Agency (FEMA 2003), the equivalent explosive charge weights may vary from 10 kg

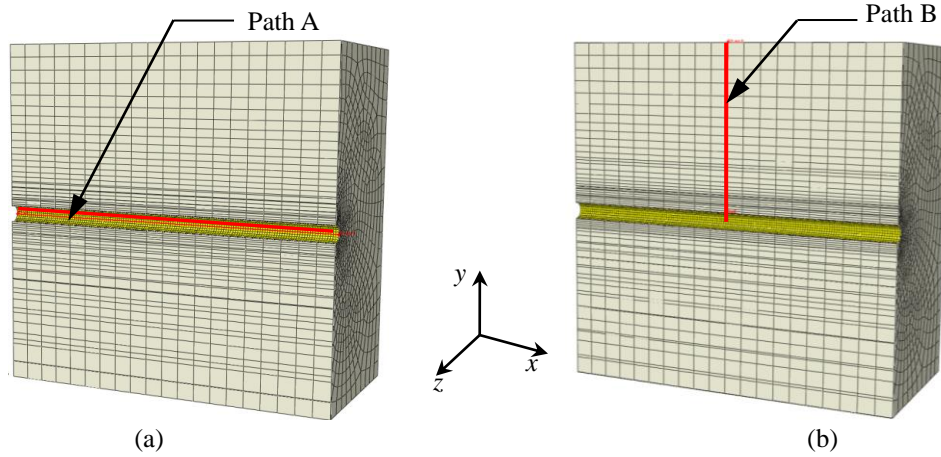


Fig. 7 Path along (a) tunnel axis and (b) tunnel crown for extraction of results

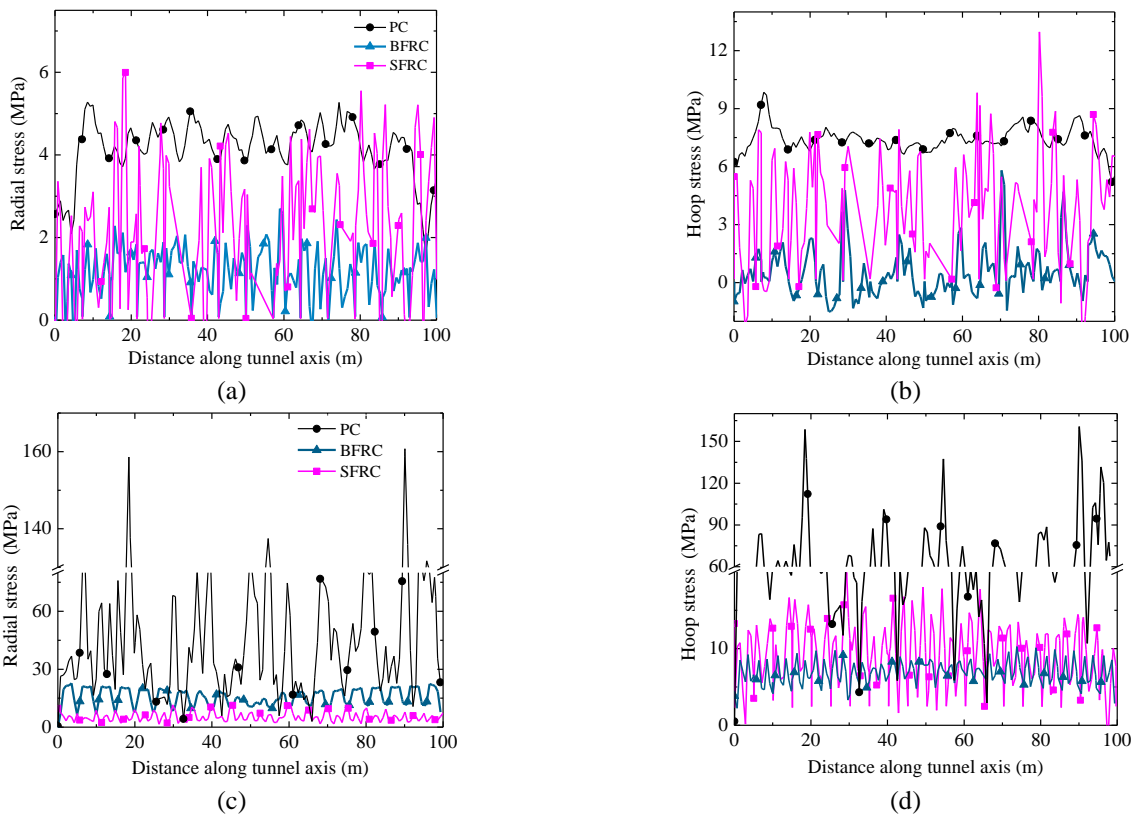


Fig. 8(a) Radial stress variation and (b) tangential stress variation for 10 kg TNT and (c) radial stress variation and (d) tangential stress variation for 50 kg TNT in different lining materials

to 50 kg TNT equivalent, which terrorists may carry with ease to underground for attacking tunnels and thus, in the present work, analyses have been performed using 10 kg and 50 kg TNT charge weights. The blast load has been calculated through hydrocode simulations assuming spherical explosive, exploding at the center of the tunnel and the load is applied on the lining surface of the tunnel in the form of pressure-time history curve. Blast load profile for different weight of explosives is obtained through couples fluid dynamics calculations using AUTODYN. It uses explicit time integration to solve the equation of motion. In the software shock wave propagation due to particular weight of explosive and its interaction with the

rigid structure is analyzed which enable the evaluation of overpressure history curve as shown in Figs. 6(a) and 6(b). For 10 kg of TNT, peak reflected blast overpressure of 2.9 MPa is observed at 0.3 mili seconds as shown in Fig. 6(a) and for 50 kg of TNT, peak reflected blast overpressure Fig. 7 Path along (a) tunnel axis and (b) tunnel crown for extraction of results of 24 MPa is observed at 0.5 mili seconds as shown in Fig. 6(b). In the present analyses, damping is not considered because it is assumed that given the blast load application time is extremely small, the damping is not activated. Figs. 7(a) and 7(b) show the paths in the domain along which the stress and displacement results have been studied. The path along the tunnel axis is

Table 4 Summary of tunnel response

Tunnel Lining Materials	Radial Stress		Response Reduction with respect to PC		Influence Zone		Response Reduction with respect to PC		Radial Displacement		Response Reduction with respect to PC	
	TNT charge weight (kg)		TNT charge weight (kg)		TNT charge weight (kg)		TNT charge weight (kg)		TNT charge weight (kg)		TNT charge weight (kg)	
	10	50	10	50	10	50	10	50	10	50	10	50
	MPa		%		m		%		mm		%	
PC	5.6	160	0	0	34	52	0	0	58	132	0	0
BFRC	3	26	46.4	83.8	20	30	40	42	20	51	65.5	140
SFRC	6	18	-7.14	88.8	25	35	25	33	36	62	37.9	121

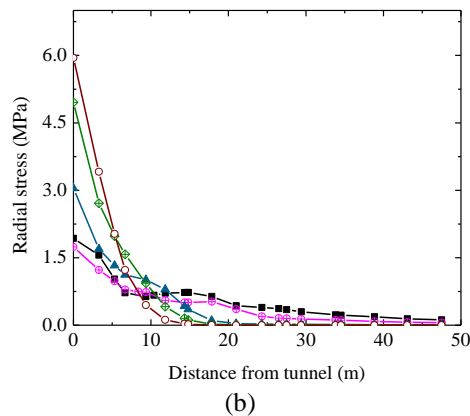
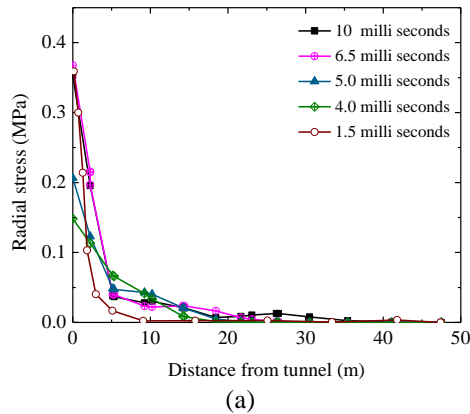


Fig. 9 Stress in rock from tunnel crown with time in BFRC for (a) 10 kg TNT and (b) 50 kg TNT

named as path A while the path perpendicular to tunnel axis is named as path B.

3. Results of blast analysis and discussion

3.1 Stress variation

Figs. 8(a) and 8(b) present the radial and hoop stresses, respectively, in the lining material along the tunnel axis path A for 10 kg TNT load. Figs. 8(c) and 8(d) show the radial and hoop stresses in the lining material along the tunnel axis path for 50 kg TNT load. Highest stresses are observed in the PC lining in both radial and tangential directions. The stresses in the SFRC lining are lesser as compared to that in the PC lining. The stresses in the BFRC lining are even lesser than that in the SFRC lining. Table 4 summarizes the

stress reductions in BFRC and SFRC linings as compared to PC lining. For 10 kg TNT load, in the radial direction the BFRC lining exhibits 46.4% less stress than that of PC lining whereas the SFRC lining exhibits 7% higher stress than that of PC lining. Similar stress variation is also observed in the hoop direction. For 50 kg TNT load BFRC lining in radial direction shows 84% less stress than that of PC lining and the SFRC lining shows 88.8% less stress than that of PC lining. Variation in hoop stress in all three lining types is observed to be similar as in the case of radial stress. Hoop stress in SFRC lining is more than that of BFRC lining as shown in Fig. 9(b). The PC lining exhibits 60% more hoop stress as compared to BFRC lining.

Figs. 9(a) and 9(b) present the results of radial stress in rock at different time instances starting from tunnel crown to the top boundary for BFRC lining along path B perpendicular to tunnel axis. Maximum stresses in rock are observed just after the loading i.e., at 1.5 milliseconds and with time, the stress reduces in rock. Effect of stress for 10 kg TNT load is not seen after 15 m from tunnel sidewall. For 50 kg TNT load, the extent of stress can be seen up to 20 m. Table 4 compares the influence zones of radial stress for PC, BFRC, and SFRC linings. The influence zone in the surroundings of PC lining for 10 kg TNT is 34 m while that for BFRC and SFRC linings are 20 m and 25 m from the tunnel boundary, respectively. Nearly 40% reduction in influence zone is observed for BFRC lining and 25% reduction in influence zone is observed for SFRC lining as compared to PC lining. For 50 kg TNT load, the influence zone in the surroundings of PC lining is 52 m while that for BFRC and SFRC linings are 30 m and 35 m from the tunnel boundary, respectively. Thus, 42% reduction in influence zone is observed for BFRC lining and 33% reduction in influence zone is observed for SFRC lining as compared to PC lining.

3.2 Displacement variation

Figs. 10(a) and 10(b) present the displacement in lining along the tunnel axis path A in radial and tangential directions for 10 kg TNT load. Figs. 10(c) and 10(d) present the displacement in lining along the tunnel axis path A in radial and tangential directions for 50 kg TNT load. Table 4 summarizes the displacement reductions in BFRC and SFRC linings as compared to PC lining. For 10 kg TNT load, radial displacement in BFRC lining is 65% less than that of PC lining and radial displacement in SFRC lining is

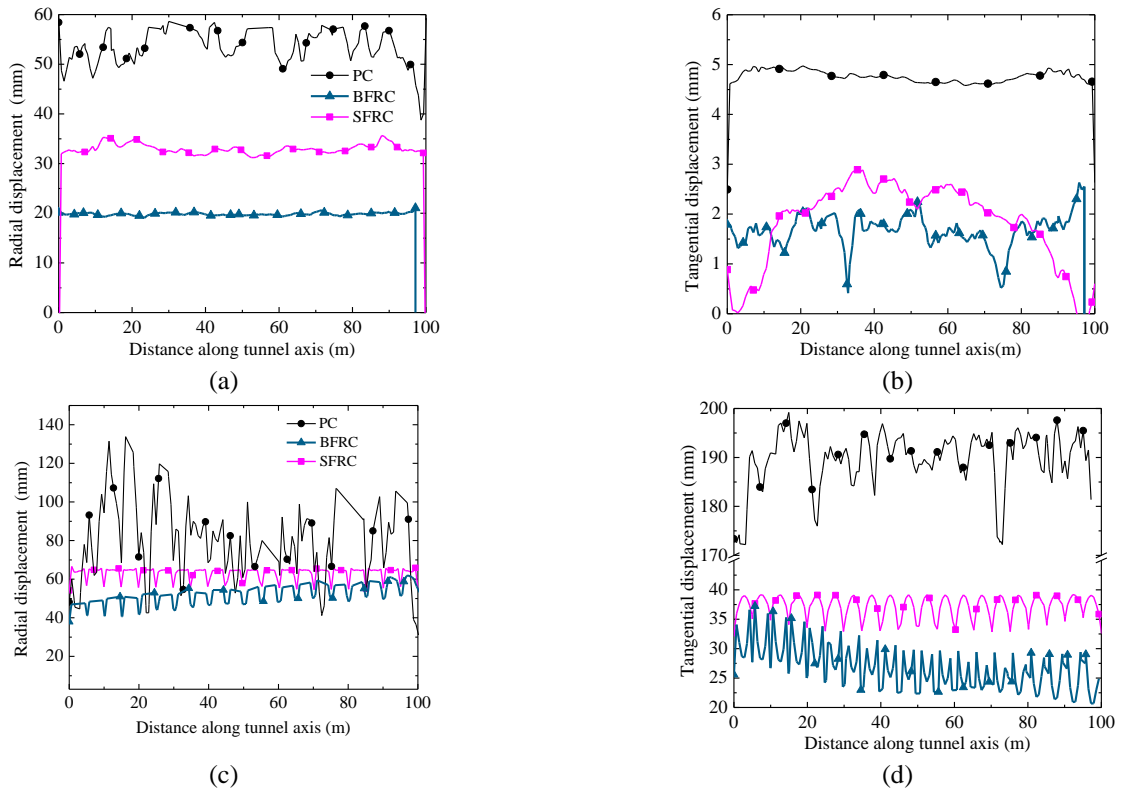


Fig. 10 (a) Radial displacement and (b) tangential displacement for 10 kg TNT and (c) radial displacement and (d) tangential displacement for 50 kg TNT in different lining materials

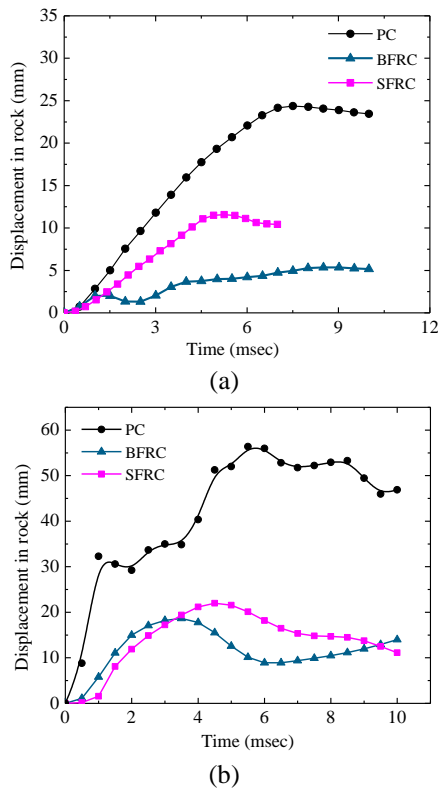


Fig. 11 Displacement time histories at tunnel crown for different tunnel lining materials

38% less than that of PC lining as shown in Fig. 10(a). Tangential displacement in BFRC and SFRC linings are

almost similar while PC lining shows maximum tangential displacement and 50% more than that of BFRC and SFRC linings as shown in Fig. 10(b). For 50 kg TNT load, the radial displacement in BFRC lining is 139% less than that of PC lining and radial displacement in SFRC lining is 120% less than that of PC lining as shown in Fig. 10(c). Tangential displacement in PC lining is 84% more than that of BFRC and SFRC linings as shown in Fig. 10(d).

The displacement time histories at the tunnel crown is computed and presented in Figs. 11(a) and 11(b) for PC, BFRC, and SFRC linings for 10 kg and 50 kg charge weights, respectively. In both the cases, it is observed that PC lining exhibits the highest displacement. For 10 kg charge weight, SFRC lining exhibits higher displacement as compared to BFRC lining whereas, for 50 kg charge weight, SFRC and BFRC linings produce comparable displacement values. Hence, for design purposes, both SFRC and BFRC linings may be recommended in the tunnel, however, it is expected that the BFRC lining will perform better as compared to the SFRC lining by exhibiting lesser displacement.

4. Conclusions

The present study investigates the performance of BFRC tunnel lining when subjected to internal blast loading and compares the performance of three different tunnel lining materials-PC, BFRC and SFRC under internal blast loading through three-dimensional nonlinear finite element analyses. The following conclusions are drawn:

- (1) For 10 kg TNT load, in the radial direction the BFRC lining exhibits 46.4% less stress than that of PC lining whereas the SFRC lining exhibits 7% higher stress than that of PC lining. For 50 kg TNT load BFRC lining in radial direction shows 84% lesser stresses than that of PC lining and the SFRC lining shows 88.8% less stress than that of PC lining. The PC lining exhibits 60% more hoop stress as compared to BFRC lining.
- (2) As compared to the PC lining, the BFRC lining exhibits 40-42% reduction in influence zone and the SFRC lining exhibits 25-33% reduction in the influence zone.
- (3) For 10 kg TNT load, the radial displacement in the BFRC lining is 65% less than that of PC lining and radial displacement in SFRC lining is 38% less than that of PC lining. For 50 kg TNT load, the radial displacement in BFRC lining is 139% less than that of PC lining and radial displacement in SFRC lining is 120% less than that of PC lining.
- (4) For design purposes, both SFRC and BFRC linings may be recommended in the tunnel for blast resistant design due to higher ductility and yield strength of BFRC and SFRC as compared to PC, however, it is expected that the BFRC lining will perform better as compared to the SFRC lining by exhibiting lesser displacement.

Acknowledgments

The research described in this paper was financially supported by the Department of Science and Technology (DST), Government of India under the project "Sensor based security and emergency management system for underground metro systems during disaster events".

References

- Abaqus V6.11 User's Manual (2011), Abaqus Inc., DS Simulia, Providence, RI, USA.
- Alam, S.M., Chakraborty, T., Matsagar, V., Rao, K.S., Sharma, P. and Singh, M. (2015), "Characterisation of Kota sandstone under different strain rates in uniaxial loading", *Geotech. Geolog. Eng.*, **33**(1), 143-152.
- Arslan, M.E. (2016), "Effect of basalt fibers on fracture energy and mechanical properties of HSC", *Comput. Concrete*, **17**(4), 553-566.
- Chakraborty, T. (2013), "Impact simulation of rocks under SHPB test", *Proceedings of the Indian National Science Academy (INSA)*, **79**(3), 1-7.
- Chakraborty, T., Larcher, M. and Gebbeken, N. (2014), "Performance of tunnel lining materials under internal blast loading", *Int. J. Protect. Struct.*, **5**(1), 83-96.
- Choi, S., Wang, J., Munfakh, G. and Dwyre, E. (2006), "3D nonlinear blast model analysis for underground structures", *Proceedings of GeoCongress*, ASCE, 1-6.
- Deshpande, V.S. and Fleck, N.A. (2000), "Isotropic constitutive model for metallic foams", *J. Mech. Phys. Solid.*, **48**, 1253-1276.
- Dong, J.K., Sirijaroonchai, K., El-Tawil, S. and Naaman, A.E. (2010), "Numerical simulation of the split Hopkinson pressure bar test technique for concrete under compression", *Int. J. Impact Eng.*, **37**(2), 141-149.
- FEMA (2003), Risk Management Series, Reference Manual to Mitigate Potential Terrorist Attacks Against Buildings, Providing Protection to People and Buildings, FEMA 426.
- Ganesan, N., Sahana R. and Indira, P.V. (2017), "Effect of hybrid fibers on tension stiffening of reinforced geopolymer concrete", *Adv. Concrete Constr.*, **5**(1), 75-86.
- Girgin, Z.C. and Yildirim, M.T. (2015), "Usability of basalt fibres in fibre reinforced cement composites", *Mater. Struct.*, **49**(8), 3309-3319.
- Hao, H., Ma, G. and Zhou, Y. (1998), "Numerical simulation of underground explosions", *Fragblast*, **2**(4), 383-395.
- Jalasutram, S., Sahoo, D.R. and Matsagar, V. (2016), "Experimental investigation on mechanical properties of basalt fibre-reinforced concrete", *Struct. Concrete*, **18**(2), 292-302.
- Khan, S., Chakraborty, T. and Matsagar, V. (2016), "Parametric sensitivity analysis and uncertainty quantification for cast iron-lined tunnels embedded in soil and rock under internal blast loading", *J. Perform. Constr. Facil.*, ASCE, **30**(6), 04016062.
- Lee, J. and Fenves, G.L. (1998), "Plastic damage model for cyclic loading of concrete structures", *J. Eng. Mech.*, **124**(8), 892-900.
- Li, W. and Xu, J. (2009), "Impact characterization of basalt fiber reinforced geopolymeric concrete using a 100-mm-diameter split Hopkinson pressure bar", *Mater. Sci. Eng. A*, **513**, 145-153.
- Liu, H. (2009), "Dynamic analysis of subway structures under blast loading", *Geotech. Geolog. Eng.*, **27**, 699-711.
- Lubliner, J., Oliver, S. and Onate, E. (1989), "A plastic damage model for concrete", *Int. J. Solid. Struct.*, **25**, 299-329.
- Mishra, S., Parashar, V., Chakraborty, T., Matsagar, V., Chandel, P., Mangla, V. and Singh, M. (2015), "High strain rate response of rocks under dynamic loading using split Hopkinson pressure bar", *PROTECT2015-5 International Workshop on Performance, Protection & Strengthening of Structures under Extreme Loading*, June, East Lansing, MI, US.
- Pawade, P.Y., Pande, A.M. and Nagarnaik, P.B. (2011), "Effect of steel fibres on modulus of elasticity of concrete", *Int. J. Adv. Eng. Sci. Technol.*, **7**(2), 169-177.
- Ramakrishnan, V., Tolmare, N.S. and Brik, V.B. (1998), "Performance evaluation of 3-D basalt fiber reinforced concrete and basalt rod reinforced concrete", Final Report for Highway IDEA Project 45, Transportation Research Board.
- Silva, P.F. and Lu, B. (2009), "Blast resistance capacity of reinforced concrete slabs", *J. Struct. Eng.*, ASCE, **135**(6), 708-716.
- Tiwari, R. (2015), "Blast response and mitigation in curved structures for underground applications", M.S. Thesis, Indian Institute of Technology (IIT) Delhi.
- Tiwari, R., Chakraborty, T. and Matsagar, V. (2014), "Dynamic analysis of underground tunnels subjected to internal blast loading", *Proceedings of the 11th World Congress on Computational Mechanics (WCCM XI)*, Barcelona, Spain.
- Tiwari, R., Chakraborty, T. and Matsagar, V. (2016), "Dynamic analysis of tunnel in weathered rock subjected to internal blast loading", *Rock Mech. Rock Eng.*, **49**(11), 4441-4458.
- Wang, Z.L., Liu, Y.S. and Shen, R.F. (2008), "Stress-strain relationship of steel fibre-reinforced concrete under dynamic compression", *Constr. Build. Mater.*, **22**, 811-819.
- Zhang, L., Sun, Y. and Xiong, W. (2015), "Experimental study on the flexural deflections of concrete beam reinforced with Basalt FRP bars", *Mater. Struct.*, **48**(10), 3279-3293.